Cell Stem Cell, Volume *30*

Supplemental Information

Generating high-fidelity cochlear organoids from human pluripotent stem cells

Stephen T. Moore, Takashi Nakamura, Jing Nie, Alexander J. Solivais, Isabel Aristizábal-Ramírez, Yoshitomo Ueda, Mayakannan Manikandan, V. Shweta Reddy, Daniel R. Romano, John R. Hoffman, Benjamin J. Perrin, Rick F. Nelson, Gregory I. Frolenkov, Susana M. Chuva de Sousa Lopes, and Eri Hashino

Figure S1

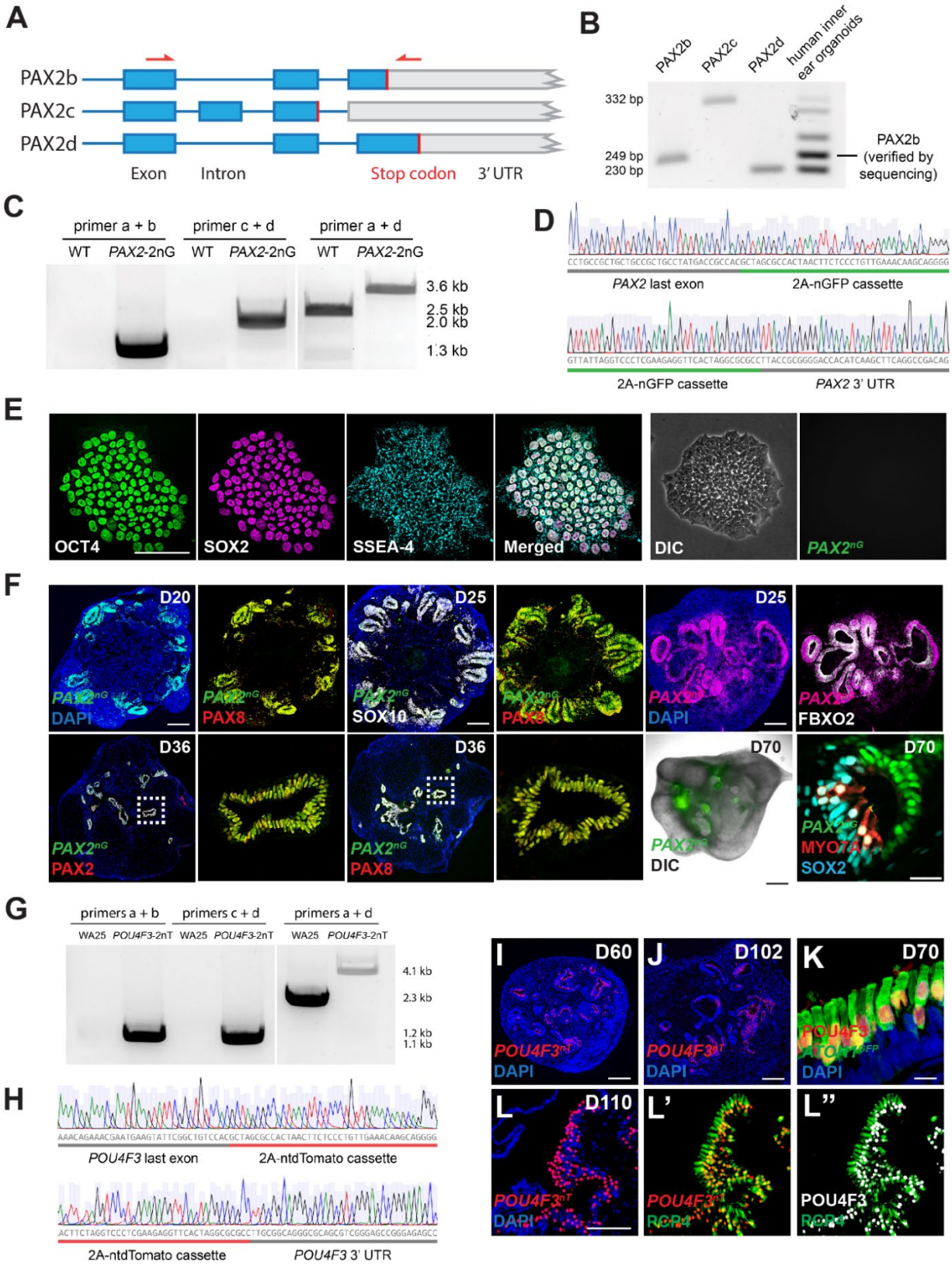
A
PAX2b
PAX2c
PAX2d
Exon
Intron
Stop codon
3′ UTR
B
PAX2b
PAX2c
PAX2d
human inner ear organoids
332 bp
249 bp
230 bp
PAX2b (verified by sequencing)
C
primer a + b
primer c + d
primer a + d
WT
PAX2-2nG
3.6 kb
2.5 kb
2.0 kb
1.3 kb
D
PAX2 last exon
2A-nGFP cassette
2A-nGFP cassette
PAX2 3′ UTR
E
OCT4
SOX2
SSEA-4
Merged
DIC
PAX2nG
F
D20
DAPI
PAX8
D25
SOX10
PAX8
D25
DAPI
FBXO2
D36
PAX2nG
PAX2
D36
PAX2nG
PAX8
D70
PAX2nG
DIC
D70
PAX2nG
MYO7A
SOX2
G
primers a + b
primers c + d
primers a + d
WA25
POU4F3-2nT
4.1 kb
2.3 kb
1.2 kb
1.1 kb
H
POU4F3 last exon
2A-ntdTomato cassette
2A-ntdTomato cassette
POU4F3 3′ UTR
I
D60
POU4F3nT
DAPI
J
D102
POU4F3nT
DAPI
K
D70
POU4F3
ATOH1nGFP
DAPI
L
D110
POU4F3nT
DAPI
L′
POU4F3nT
RORB
L″
POU4F3
RORB

Figure S1. Generation and validation of *PAX2*^{nG}/*POU4F3*^{nT} reporter hESC lines, Related to Figure 1.

(A-B) Schematic of PAX2 isoforms (A) and RT-PCR data showing that PAX2b is the most abundant isoform expressed in stem cell-derived inner ear organoids (B).

(C-D) PCR amplification using primer sets shown in (Figure 1A) demonstrated bi-allelic insertion of the 2A-nGFP cassette at the *PAX2* locus (C), which was confirmed by Sanger sequencing (D).

(E) Immunofluorescence of undifferentiated *PAX2*^{nG} hESCs reveals the expression of multiple pluripotency markers and absence of constitutive *PAX2*^{nG} reporter expression.

(F) Representative immunohistochemistry of sectioned *PAX2*^{nG} hESC-derived inner ear organoids reveals expression of *PAX2*^{nG} localized to epithelial vesicles that co-express otic markers PAX8 by D20, as well as SOX10 and FBXO2 by D25. Expression of *PAX2*^{nG} is sustained and can be detected by live imaging at D70. SOX2/MYO7A+ hair cells can be detected on the luminal surface of *PAX2*^{nG}+ vesicles at D70.

(G-H) PCR amplification of the *POU4F3* locus reveals bi-allelic insertion of the 2A-ntdTomato reporter cassette (G). Sanger sequencing reveals correct insertion and orientation of the reporter cassette immediately downstream of the *POU4F3* stop codon (H).

(I-J) *POU4F3*^{nT} reporter expression is confined to cells on the luminal surface of vesicles at D60 (I) and 100 (J).

(K) POU4F3 expression confirms faithful *POU4F3*^{nT} reporter expression. (L-L") Immunohistochemistry of D110 inner ear organoids derived from *POU4F3*^{nT} hESCs reveals that tdTomato+ puncta label the nuclei of PCP4+ hair cells and perfectly colocalize with antibody-labeled POU4F3.

Scale bars, 50 μm (E), 200 μm (F, G, H), 10 μm (K),100 μm (L).

Figure S2

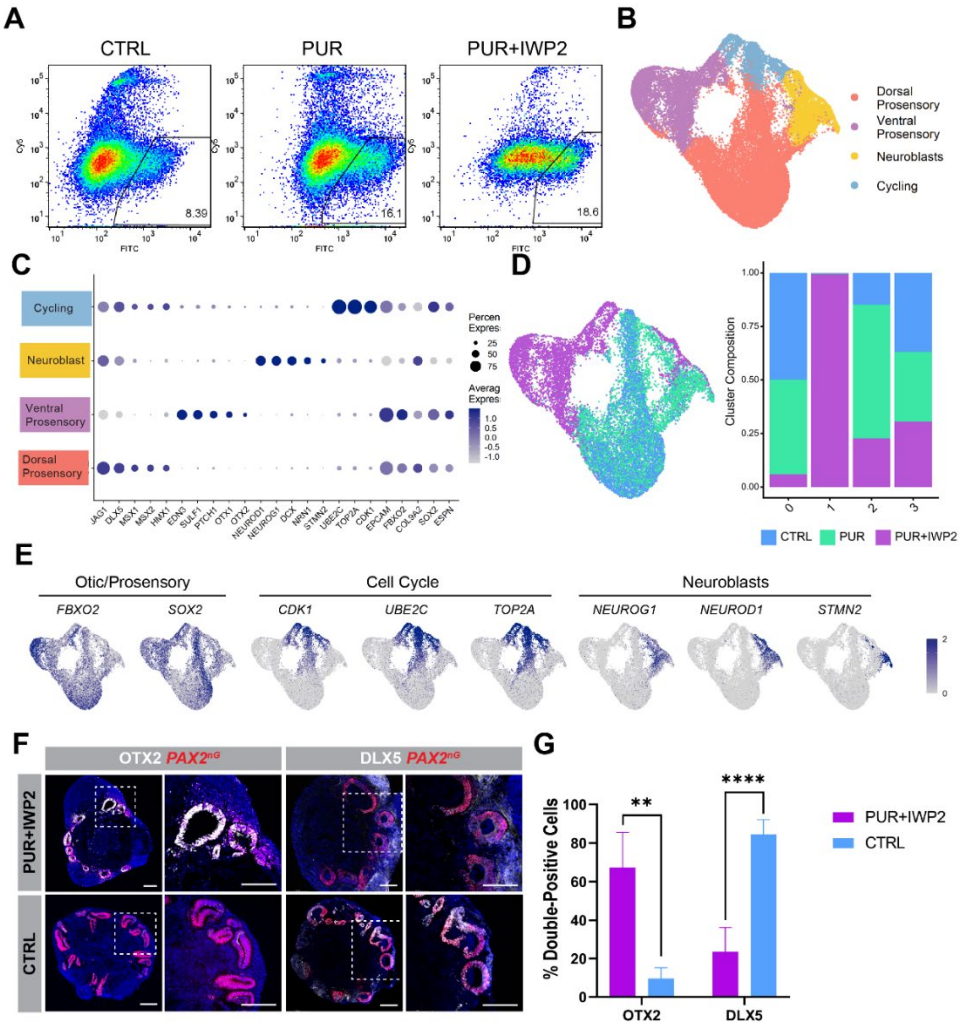

Figure S2. scRNA-seq analysis of *PAX2*^{nG} cells in D20 CTRL, PUR, and PUR+IWP2 inner ear organoids, Related to Figure 3.

(A) FACS gating strategy used to isolate *PAX2*^{nG}+ cells from whole aggregates. Propidium iodide was used as a viability dye (Cy5).

(B) Cell clusters were generated by Seurat and visualized using UMAP.

(C) Dot plot showing the relative expression of marker genes within annotated clusters.

(D) Feature plots show canonical markers of otic progenitors, neuroblasts, and cycling cells.

(E) Colored cells show the distribution of conditions within each cluster. A stacked histogram shows the composition of each cluster by condition. The numbers of sequenced cells: 12,213 (CTRL), 13,077 (PUR), 11,784 (PUR+IWP2). The number of cells after QC filtering: 11,199 (CTRL), 11,933 (PUR), 10,755 (PUR+IWP2).

(F) Representative immunohistochemistry of D25 organoid sections reveals differential expression of OTX2 and DLX3 between conditions.

(G) Quantitative comparison of OTX2 and DLX3 expression between PUR+IWP2 and CTRL conditions by immunohistochemistry; n = 5 biological samples from separate experiments per group; Welch's two-sided *t*-test ** P<.001; ***P<0.0001; values are mean ± SEM.

Scale bars, 200 μm.

Figure S3

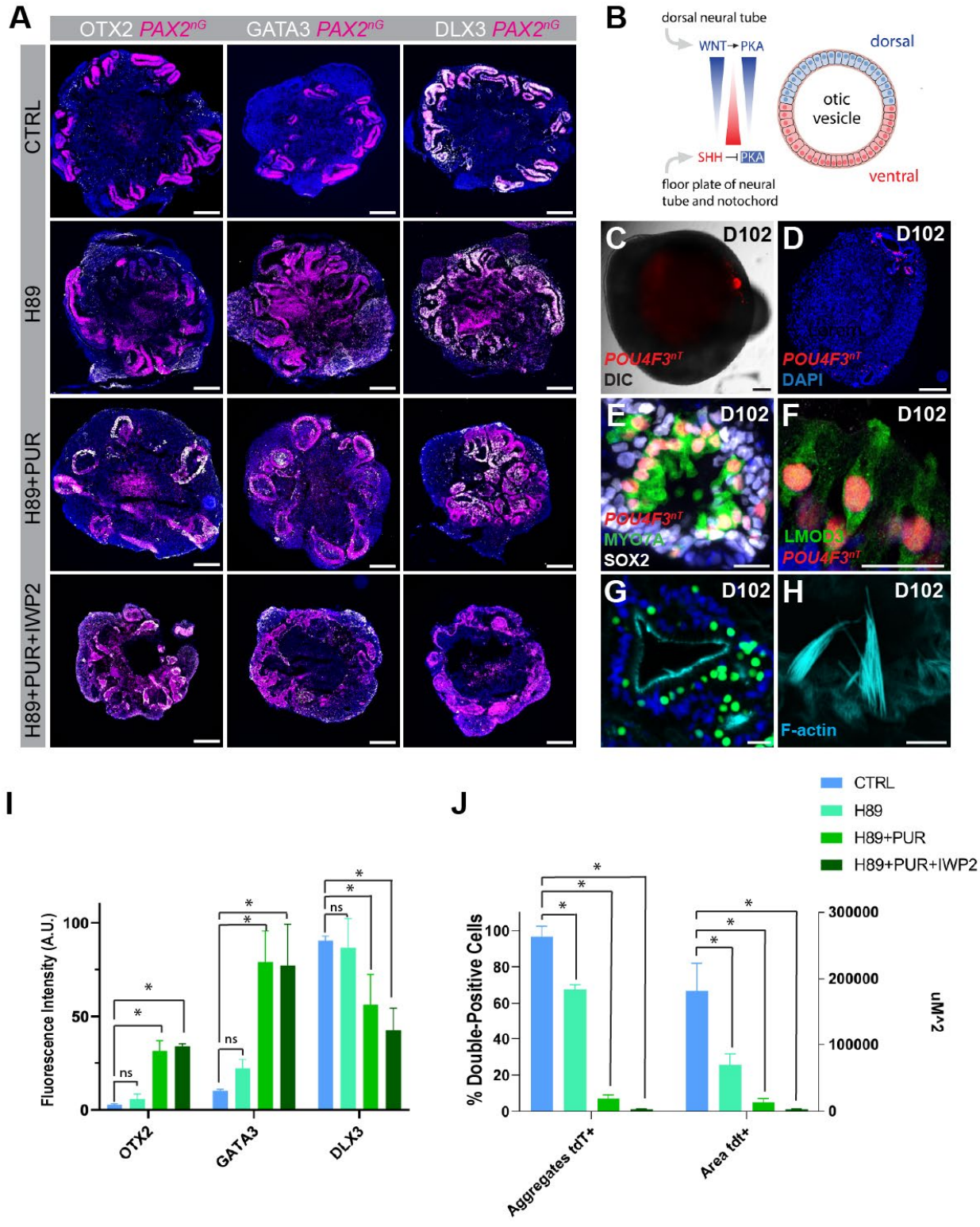
A
OTX2 PAX2nG
GATA3 PAX2nG
DLX3 PAX2nG
CTRL
H89
H89+PUR
H89+PUR+IWP2
B
dorsal neural tube
WNT→PKA
SHH⊣PKA
floor plate of neural tube and notochord
otic vesicle
dorsal
ventral
C D102
POU4F3nT
DIC
D D102
POU4F3nT
DAPI
E D102
POU4F3nT
MYO7A
SOX2
F D102
LMOD3
POU4F3nT
G D102
H D102
F-actin
I
Fluorescence Intensity (A.U.)
100
50
0
ns
OTX2
GATA3
DLX3
J
CTRL
H89
H89+PUR
H89+PUR+IWP2
% Double-Positive Cells
100
80
60
40
20
0
300000
200000
100000
0
uM^2
Aggregates tdT+
Area tdt+

Figure S3. Protein Kinase A inhibition fails to promote hair cell differentiation, Related to Figure 3.

(A) Representative immunohistochemistry of the regionally expressed otic markers OTX2, GATA3, and DLX3 for D25 inner ear organoids treated with or without 10 μM H89 alone or in combination with PUR or PUR+IWP2.

(B) Schematic illustration of the proposed role of H89 in the SHH pathway.

(C) Live image of a D102 cell aggregate treated with H89 and PUR shows a single *POU4F3*^{nT}+ inner ear organoid.

(D) Representative image of a D102 PUR+H89-treated aggregate showing a small number of *POU4F3*^{nT}+ puncta.

(E) Immunohistochemistry of a D102 inner ear organoid treated with H89+PUR shows MYO7A+ hair cells with *POU4F3*^{nT}+ nuclei on the luminal surface of SOX2+ epithelium.

(F) Confocal image of a hair cell in a H89+PUR-treated organoid shows detectible expression of the cochlear outer hair cell marker LMOD3.

(G-H) Immunohistochemistry of D102 H89+PUR-treated inner ear organoids stained with phalloidin reveals hair bundles with vestibular-like length and morphology.

(I) Quantitative comparison of OTX2, GATA3 and DLX3 expression among different treatment groups; n = 5 biological samples from separate experiments per group; *P<0.01; values are mean ± SEM.

(J) Quantitative comparison of the percentage of tdTomato expressing aggregates (left y-axis), and total tdTomato positive area per aggregate (right y-axis) among different treatment groups; n = 12 biological samples from separate experiments per group; One-way ANOVA with Tukey's multiple comparisons test *P<0.01; ns, not significant; values are mean ± SEM.

Scale bars, 200 μm (A-D), 20 μm (E-G), 5 μm (H).

Figure S4

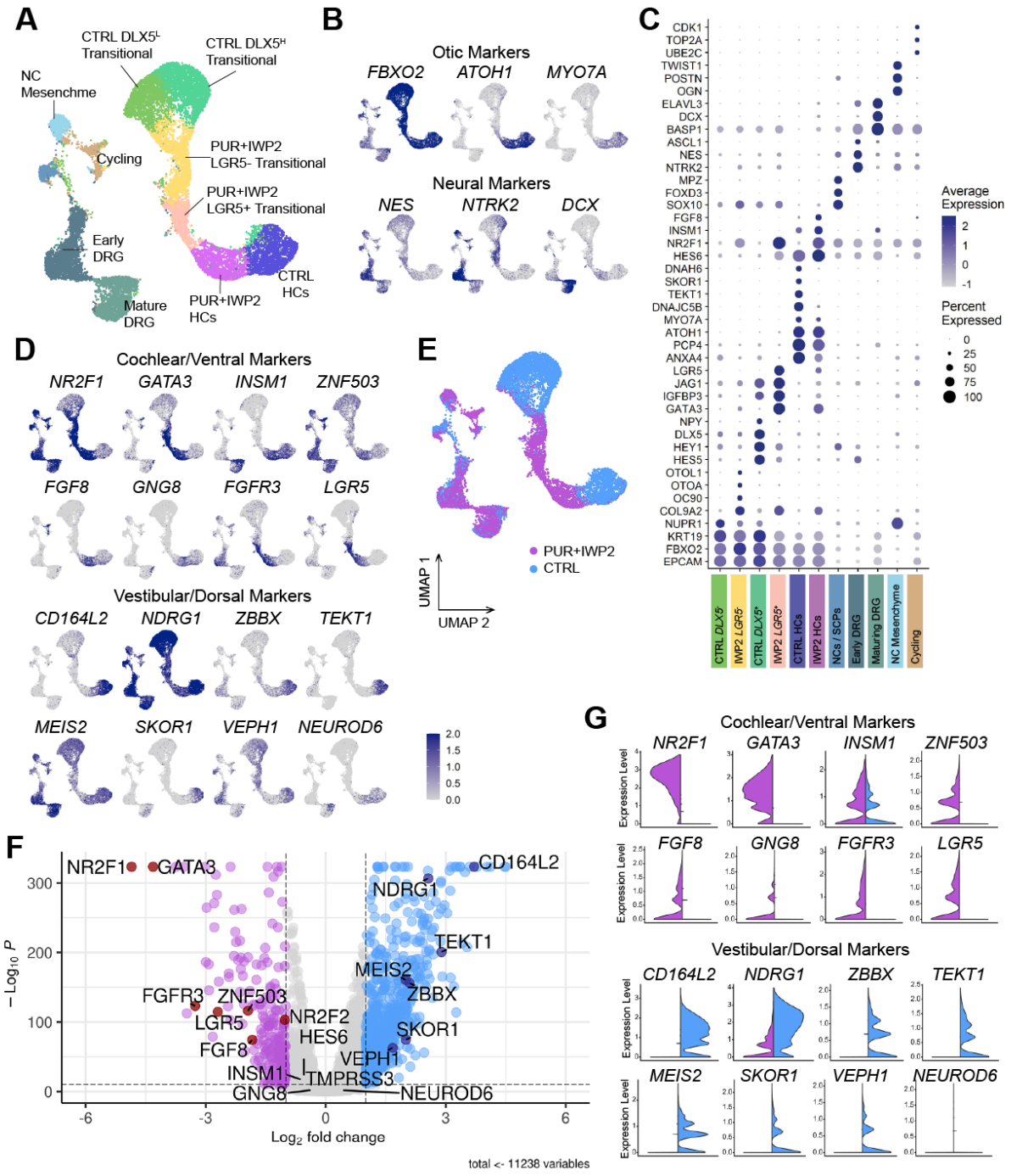

Figure S4. scRNA-seq analysis of FACS-sorted *POU4F3*^{nT}+ cells in D80 CTRL and PUR+IWP2 inner ear organoids, Related to Figures 4 and 5.

(A) UMAP projections showing annotated clusters of *POU4F3*^{nt}+ cells.

(B) Feature plots showing the distributions of inner ear and neural marker genes.

(C) Dot plot showing the relative expression of marker genes within annotated clusters.

(D) Feature plots showing the distribution of cochlear/ventral markers and vestibular/dorsal marker genes.

(E) UMAP plot grouped by experimental conditions. The estimated number of sequenced cells: 14,198 (CTRL), 13,403 (PUR+IWP2). The number of cells after QC filtering: 8,702 (CTRL), 8,966 (PUR+IWP2).
(F) Volcano plot depicting differentially expressed genes between PUR+IWP2 and CTRL hair cells shown in magenta and blue, respectively.
(G) Violin plots showing differentially expressed cochlear and vestibular genes between PUR+IWP2 and CTRL hair cells shown in magenta and blue, respectively.

Figure S5

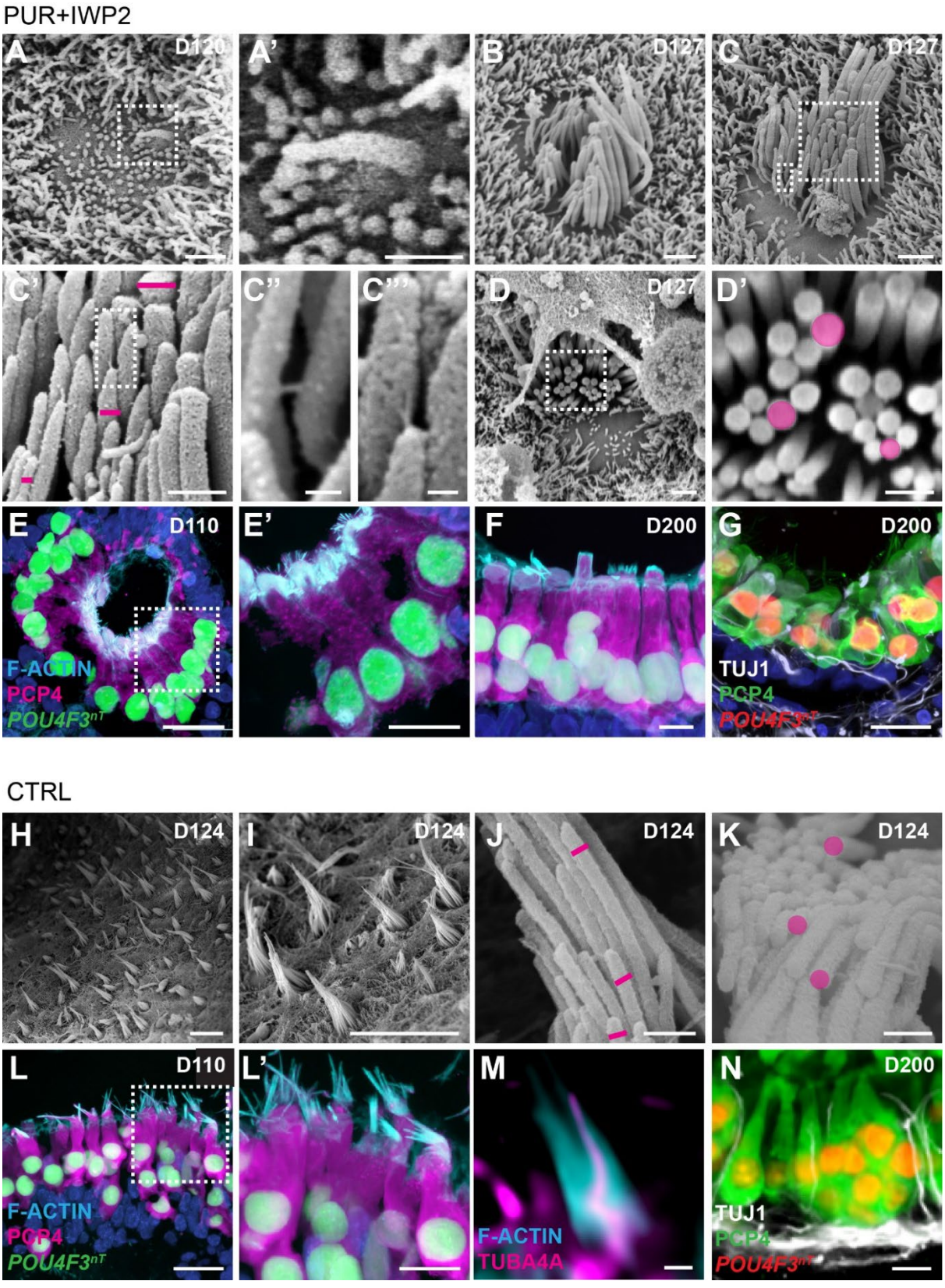
PUR+IWP2
A
D120
A'
B
D127
C
D127
C'
C''
C'''
D
D127
D'
E
D110
E'
F
D200
G
D200
F-ACTIN
PCP4
POU4F3nT
TUJ1
PCP4
POU4F3nT
CTRL
H
D124
I
D124
J
D124
K
D124
L
D110
L'
M
N
D200
F-ACTIN
PCP4
POU4F3nT
F-ACTIN
TUBA4A
TUJ1
PCP4
POU4F3nT

Figure S5. Hair cells in PUR+IWP2 and CTRL inner ear organoids exhibit distinctive hair bundle morphology, Related to Figure 6.

(A-C’’’) Scanning electron micrographs of hair bundles from PUR+IWP2 treated cells shows developmental progression of hair bundle organization including the assembly of tip links.

(D-D’) Scanning electron micrographs showing increasing diameter of stereocilia on the apical surface of a PUR+IWP2 hair cell.

(E-F) Confocal microscopic images showing short F-actin+ stereocilia on the apical surface of PUR+IWP2 treated hair cells at D110 and -200.

(G) TUJ1+ neurite processes contacting PUR+IWP2 hair cells at D200.

(H-K) Scanning electron micrographs of CTRL hair bundles reveal long pointed morphologies with consistent-diameter stereocilia within each hair bundle.

(L-L’) Confocal microscopic images show long, pointed F-actin+ stereocilia on the surface of CTRL hair cells.

(M) TUBA4A-positive kinocilium on the apical surface of a CTRL hair cell.

(N) TUJ1+ neurite processes contacting CTRL hair cells at Day-200.

Scale bars, 1 μm (A-D, M), 500 nm (A’, C’, D’, J, K), 100 nm (C’’, C’’’), 10 μm (E’, H, I, L’, N), 20 μm (E, F, G, L).

Figure S6

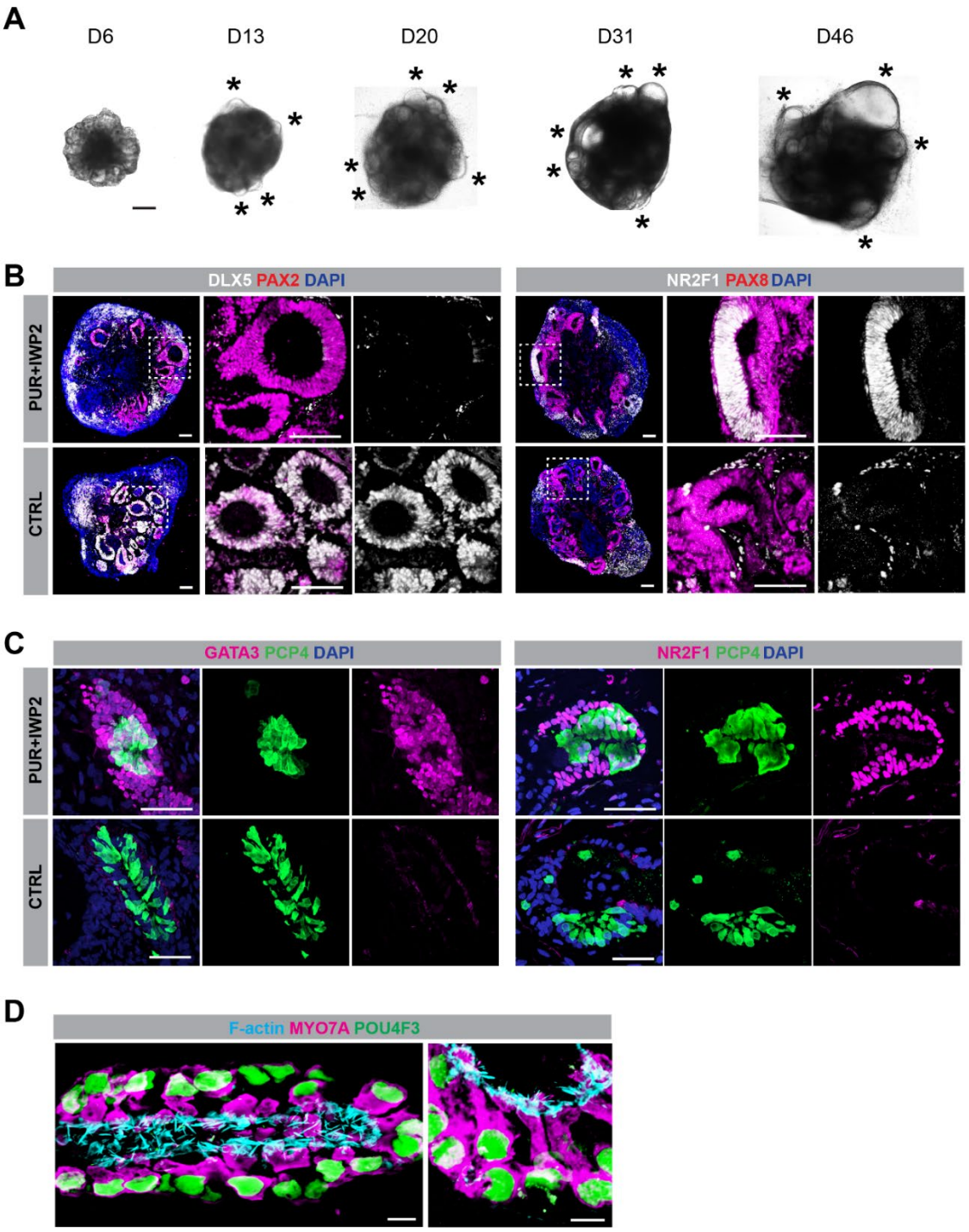

Figure 6. Human iPSCs differentiate into cochlear organoids in the presence of PUR and IWP2, Related to Figures 3, 5 and 6.

(A) Live DIC images of whole aggregates containing multiple vesicles (asterisks) at different time points after the start of differentiation.

(B) Representative images of D25 samples show notably lower expression of DLX5 and higher expression of NR2F1 in PAX2/PAX8-positive cells of PUR+IWP2 organoids vs. CTRL organoids.
(C) Representative images of D82 samples show notably higher expression of GATA3 and NR2F1 in PUR+IWP2 organoids vs. CTRL organoids.
(D) Confocal microscopic images of PUR+IWP2-treated hair cells exhibiting short F-actin^{+} hair bundles.
Scale bars, 250 μm (A), 100 μm (B), 50 μm (C), 10 μm (D).

Figure S7

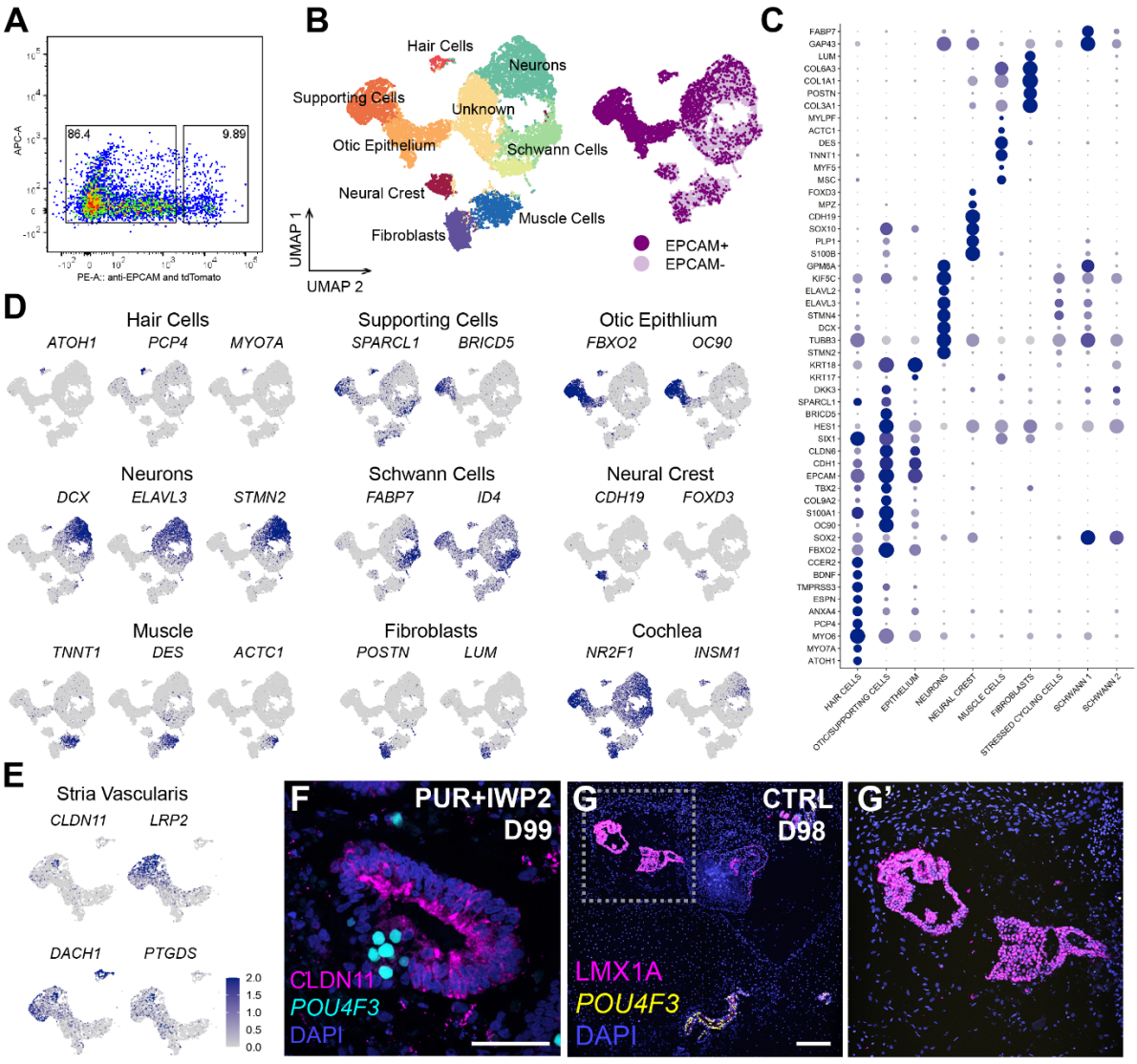

Figure S7. scRNA-seq analysis of EPCAM-positive and -negative cells isolated from D81 PUR+IWP2 organoids suggests the presence of peripheral neurons, Schwann cells and stria vascularis, Related to Figures 4 and 5.

(A) FACS gating strategy used to isolate EPCAM+/- cells from dissociated organoid cells.
(B) UMAP plot and cluster annotation of merged datasets and UMAP plot grouped by EPCAM-positive and -negative cells. The total number of sequenced cells: 7,789 (EPCAM+), 14,487 (EPCAM-). The number of cells after QC filtering: 7,702 (EPCAM+), 13,290 (EPCAM-).
(C) Dot plot of cluster marker genes.
(D) Feature plots for cluster marker genes.
(E) Feature plots for stria vascularis marker genes.
(F) CLDN11, a stria vascularis marker, is localized on the luminal surface of a vesicle containing *POU4F3*+ hair cells in a D99 PUR+IWP2 organoid.
(G-G') LMX1A, an endolymphatic duct marker, is present in ductal structures of a D98 CTRL organoid.
Scale bars, 50 µm.

Table S1

A

Off-target site	Chr.	Strand	Position	Sequence	# of mismatches	Score	Gene	Off-target indels / mutations?
1	chr3	1	135493203	AGACCTGCACTAGCTACCGAAG	4	0.279869	None	No
2	chr20	1	34638629	ACGGCCGCCATTAGTCACCGAGG	4	0.148505	NR_027451	No
3	chr15	-1	87289949	ATGACCAACACTAGATACAGTGG	4	0.086671	None	No
4	chr6	1	146607891	ATGACCTCCACAAGTTACAAAAG	4	0.067489	None	No
5	chr1	1	8674055	AGGACCACCACTAGTAACAGAGG	4	0.060751	None	No
6	chr15	-1	22578882	AGGACCACCACTAGTAACAGAGG	4	0.060751	None	No
7	chr19	1	39591440	ATGGCCGCCACTTGGTACAGAGG	4	0.051728	NM_001004318	No
8	chr1	-1	111029471	ATGACCTCCACTAGGTCCTGCAG	4	0.033368	NR_003599	No
9	chrX	1	122689718	ATGACCTCCACTAATTCCCTGGG	4	0.024981	None	No
10	chr3	1	177870333	GTGACCGCCACTAGTGATCACGG	4	0.023962	None	No

B

Off-target site	Chr.	Strand	Position	Sequence	# of mismatches	Score	Gene	Off-target indels / mutations?
1	chr2	1	16391400	GTTCTGCTTTCCACTGATTGGAG	3	1.632771	None	No
2	chr3	-1	188314251	AGTTGTCTGTCCACTGATTGTAG	3	1.468072	None	No
3	chr12	-1	101614310	TCTCTGCTGTCCACTGATTTAAG	4	0.710795	None	No
4	chr4	1	53847222	TTTCTGCGGTCCACTGATTTAAG	4	0.710795	None	No
5	chr18	1	68394376	AGTTAGCTGTCCACTGATTCAGG	4	0.697447	None	No
6	chr11	1	128463498	ATGCAGCAGTCCACTGATTACAG	4	0.675007	None	No
7	chr2	1	152741440	AATCTGCTGTCCACTGAGTGGGG	3	0.65679	None	No
8	chr8	1	93202010	GGTCTGCTGTCCGCTGATTGTGG	4	0.581725	None	No
9	chr1	-1	194082508	TTTCTGCTGGCCACTGGTTGAAG	4	0.571588	None	No
10	chr9	-1	8278749	TTTCTTATGTCCACTGATTGGAG	4	0.564015	None	No

C

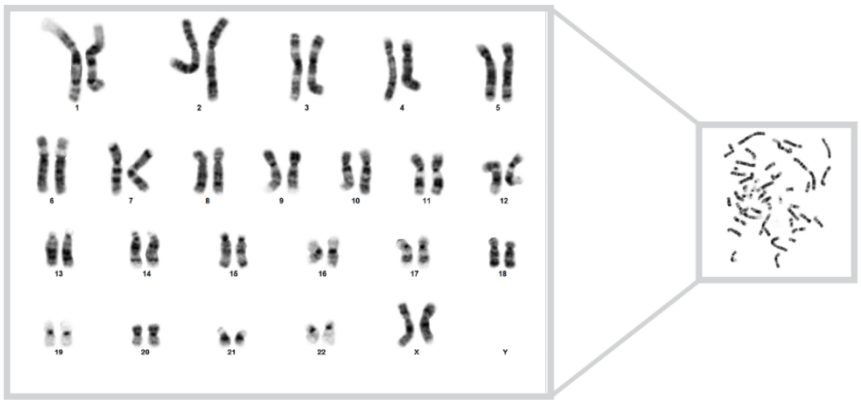

Table S1. Characterization of the *PAX2*^{nG}/*POU4F3*^{nT} reporter hESC line established in this study, Related to Figure 1.

(A-B) Sequencing results for the top 10 predicted off-target CRISPR sites for *PAX2* (A) and *POU4F3* (B) reveal no insertions or deletions in the surrounding loci.

(C) The *PAX2*^{nG}/*POU4F3*^{nT} hESC line exhibits normal karyotyping results.

Table S2

PAX2 left homology arm Fwd: GGTACCTTTCCACCCATTAGGGGCCATGC
PAX2 left homology arm Rev: GCTAGCGTGGCGGTCATAGGCAGCG
PAX2 right homology arm Fwd: GGCGCGCCTTACCGCGGGGACCACATCA
PAX2 right homology arm Rev: TCTAGAGCCAGCTCAGAACCGGTTCTTACC
POU4F3 left homology arm Fwd: GGTACCATGACCTGGGCTTTGAGGAGAGG
POU4F3 left homology arm Rev: GCTAGCGTGGACAGCCGAATACTTCATTCGTTTCTG
POU4F3 right homology arm Fwd: GGCGCGCCTTGCGGCAGGGCGC
POU4F3 right homology arm Rev: TCTAGATAAATAATAGTAATGAACGATGTTAACAACAACAGTAATAACAAAAGTGCAAGG

Table S2. Primers used to construct PAX2 and POU4F3 donor vectors, Related to Key Resources Table.